Coulombic and pre-Coulombic geometry evolution of carbonyl sulfide in an intense femtosecond laser pulse, determined by momentum imaging

J. H. Sanderson*
Department of Physics, University of Waterloo, Waterloo, Ontario, Canada N2L3G1

T. R. J. Goodworth, A. El-Zein, W. A. Bryan, and W. R. Newell†
Department of Physics and Astronomy, University College London, Gower Street, London WC1E 6BT, United Kingdom

A. J. Langley and P. F. Taday
Central Laser Facility, Rutherford Appleton Laboratory, Chilton, Didcot, Oxfordshire OX11 0QX, United Kingdom
(Received 22 November 2001; published 19 March 2002)

The Coulomb explosion of OCS in laser pulses of 55 fs and peak intensity of 2×10^{15} W cm^{-2} has been investigated using an ion-momentum imaging technique to determine the shape of the exploding molecule. The results, which are interpreted using a generalized, classical, enhanced ionization model show a range of geometries consistent with earlier measurements on CO_2, exhibiting an enhancement of the bond angle, but no appreciable straightening. Consideration of the pre-Coulombic motion improves the agreement of our results with the enhanced ionization model, whilst revealing the presence of increased molecular bending.

DOI: 10.1103/PhysRevA.65.043403 PACS number(s): 42.50.Hz, 33.80.Gj, 33.80.Wz

I. INTRODUCTION

Recent momentum imaging experiments with femtosecond laser pulses [1,2] have shown that, during Coulomb explosion, linear triatomic molecules display geometric modification outside the range allowed by the zero-point motion of the neutral molecule. First, the bond lengths observed are around double that of the neutral molecule, indicating that enhanced ionization has taken place during molecular dissociation [3,4]. Second, a mixture of straightened and bent geometries have been observed.

It would be desirable to be able to read a set of momentum maps as a direct molecular image. In order to do this for a triatomic molecule, the pattern of momentum displayed by the central ion is crucial. Conservation of momentum restricts the amount of kinetic energy central ions can receive during Coulomb explosion. Indeed, in the ideal case of a straight, symmetric molecule dissociating via a symmetrical dissociation channel the energy, and thus momentum, of the central atomic ion will be zero. A strong signal at zero momentum on the central-ion map would indicate a bond-angle distribution peaked at 180°. Such an interpretation ignores the effect of detector acceptance angle, which causes low-momentum ions produced by a molecule with a small bend (170° for instance) to be detected when their initial trajectory is not towards the detector. As the detector only measures the component of momentum parallel to the time-of-flight (TOF) axis, this gives rise to an experimentally enhanced signal at zero momentum. In order to counter this the corrected momentum-imaging technique was developed [5], which removes the effect of the finite collection angle and, in doing so, corrects for the enhanced signal near zero momentum. The details of this technique have been described previously [1] and so will not be repeated here. The advantage of this approach is the directness with which molecular geometry can be inferred; a set of experimental momentum maps can be compared directly with maps derived from the simulation of molecular Coulomb explosion. The alternative approach is to compare the experimental momentum maps with those generated by first simulating the Coulomb explosion of a molecule, and then allowing the molecular fragments to propagate through a simulation of the spectrometer [6,7]. Ultimately, this alternative technique, which will be referred to as the uncorrected method, should yield the same geometry information as the corrected method. A possible disadvantage of the corrected method is that the magnitude of the correction applied may affect the molecular geometry observed.

In its ground vibrational state, neutral carbon dioxide has an equilibrium angle of 175° and zero probability of 180° due to a degeneracy of the normal modes of vibration [8–10] that are always present as zero-point motion. Recent experimental work has provided contradictory evidence of deformation in an intense laser field: Using a corrected momentum-imaging technique [1], Bryan *et al.* have observed a broadening of the bond-angle distribution to 150° with no enhancement in the distribution near 180°. Conversely, the use of an uncorrected momentum-imaging technique [2] has given rise to the observation that the peak in the bond angle distribution lies at 180° with the range of bond-angles reaching 150°. In a previous study H_2O was shown to straighten during laser-induced dissociation and Coulomb explosion [5] using the corrected momentum-mapping technique. This was recently confirmed [6] by measurements made using the uncorrected method. This agreement is a good indication that the magnitude of correction used was appropriate. Nevertheless, in the case of linear triatomic molecules, it would be advantageous to examine a

*Electronic address: j3sander@scimail.uwaterloo.ca
†Electronic address: w.r.newell@ucl.ac.uk

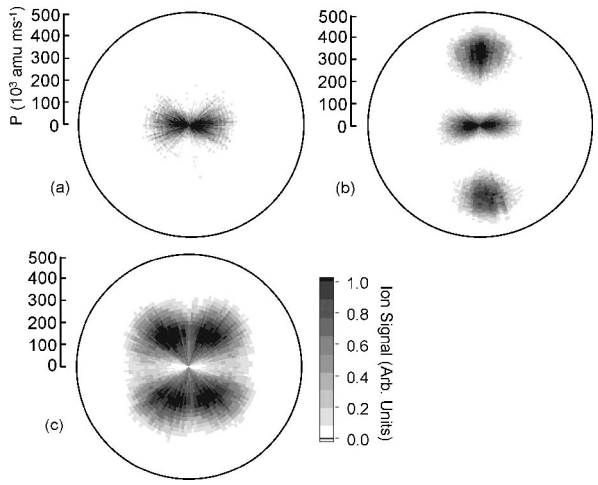

FIG. 1. Uncorrected momentum maps showing (a) C^{3+} from CO_2, (b) N^{3+} from N_2O, and (c) C^{3+} from OCS. Laser polarization axis vertical in page.

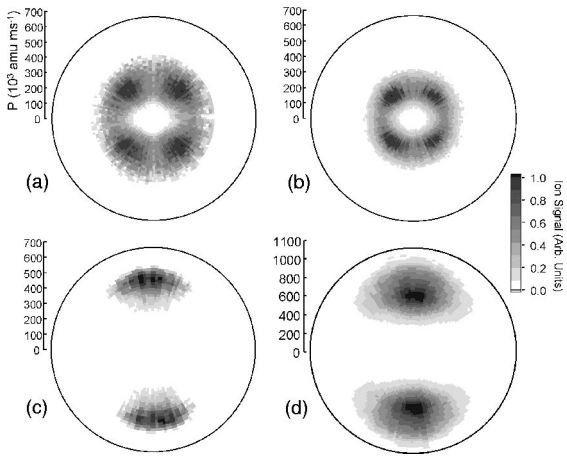

FIG. 2. OCS experimental momentum maps corrected for detector collection efficiency (a) C^{3+}, (b) C^{2+}, (c) O^{3+}, and (d) S^{4+}. Laser polarization axis vertical in page.

system that requires less extensive correction to its momentum maps. This would allow us to reliably examine the issue of straightening. To do this we must examine the geometry of a molecule that does not possess the center-of-mass inversion of CO_2. In consequence, the middle-ion fragment will be ejected with increased momentum, reducing the relative significance of the correction applied to the momentum maps. Possible asymmetric molecular subjects that satisfy this requirement are N_2O and OCS, of which OCS is the more asymmetric. Figure 1 shows a comparison of the uncorrected momentum maps for C^{3+} from CO_2 [1], N^{3+} ions from N_2O, and the C^{3+} from OCS. As discussed above, the C^{3+} signal from CO_2 is centered at zero momentum and has a ''bowtie'' geometry which suggests that, even before the data is corrected, the molecule possesses on average a slightly bent geometry. The N^{3+} momentum map consists of components from the end and middle ions and illustrates how the molecular alignment and geometry is reflected strikingly in the fragment ion momentum. The end ions acquire most of the energy released in the Coulomb explosion and their momentum is projected in the direction of the laser polarization. Conversely, the middle ion acquires only a small momentum but moves perpendicularly to the laser polarization due to the molecular bend. The fact that there is signal both above and below the central momentum island ion simply implies that there is no preferential alignment between NNO and ONN. The momentum map of the middle N ion is similar in shape to the C ion from CO_2 and has a bowtie appearance, again suggesting a slightly bent geometry. The C^{3+} ion from OCS possesses a quite different momentum map, unique in the triatomic molecules examined so far by momentum imaging (CO_2 [1], H_2O [5,6], and SO_2 [7]) in which four distinct lobes are visible with maximum signal at around 150 (10^3 amu ms^{-1}). This pattern is to be expected as OCS is asymmetrical and so conservation of momentum, even for a perfectly straight molecule, would result in a nonzero momentum for the middle ion. The relatively high momentum of the central fragment ion from OCS means that it is an excellent candidate for closer inspection, as the amount of correction necessary is much smaller than for the middle ion from either CO_2 or N_2O.

II. EXPERIMENTAL CONFIGURATION

The experimental system and laser used were similar to that described earlier [1], and so will only be described briefly. Pulses of 950 μJ with a wavelength of 790 nm and pulse length of 55 fs were used from the 10 Hz ASTRA Ti:sapphire laser at the Rutherford Appleton laboratory. The incident laser beam enters the vacuum system, which has a base pressure of 10^{-9} Torr, through a fused silica window and is reflection focused using an $f/5$ spherical mirror into the interaction region giving a near-diffraction-limited spot size, calculated to be 12 μm. The intensity was calculated from the spot size and the pulse energy to peak at 2×10^{15} W cm^{-2}. The laser focus was situated in a central plane equidistant from two parallel grids separated by 20 mm, which formed the source region of a Wiley-McLaren-type TOF mass spectrometer [11]. A 3-mm aperture was placed in front of the microchannel plates to improve angular resolution [5]. During the experiment the target gas pressure rose to 10^{-7} Torr. The signal from the channel plates was fed directly into a Tektronix TDS 744A digital oscilloscope interfaced to a personal computer. The laser pulses were monitored as previously [1] in order to minimize the effect of energy fluctuations. The polarization was rotated in 2° steps with a time-of-flight spectrum recorded at each step. Only 100 laser pulses were needed to build up each spectrum, so a two-dimensional matrix of TOF spectra from 0° to 360°, subsequently used to construct the ion-momentum maps, could be built up in approximately 30 min.

III. RESULTS AND ANALYSIS

Figure 2 shows corrected momentum maps for the fragment ions from an ensemble of channels, of which the (3,3,4) channel of OCS is a strong component. The notation (Q_1,Q_2,Q_3) represents the fragmentation channel, i.e., $(O^{Q_1+},C^{Q_2+},S^{Q_3+})$. As expected the O and S ions, ejected

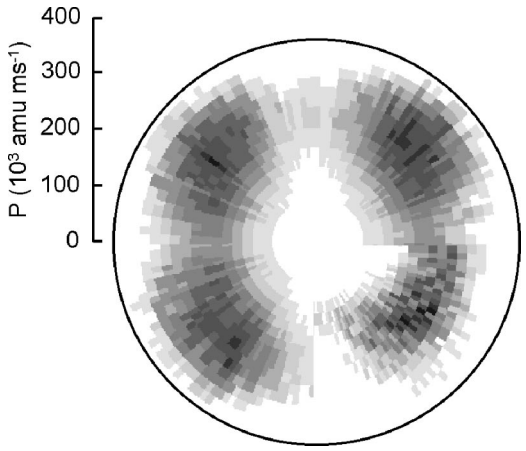

FIG. 3. C^{3+} ion momentum map from the Coulomb explosion of OCS. Simulated map shown in lower right quadrant. Experimental results taken under a 600 V cm^{-1} extraction field.

from the end of the molecule, possess the largest momenta and have trajectories along the polarization direction. The corrected C^{3+} ion map now has a more distinct four-lobe structure that can be modeled in conjunction with the O and S ions to find likely molecular geometries. This procedure, described in detail recently [1], consists of first determining the dominant dissociation channels from a covariance map experiment [12] and subsequently using Monte Carlo techniques to generate momentum maps from model Coulomb explosion geometry and alignment distributions. The best distributions are then derived by a least-squares comparison with the experimental data. A comparison between one quadrant of the generated momentum map and three quadrants of the experimental map for C^{3+} from OCS is shown in Fig. 3. The simulation was derived from a combination of channels; (2,3,3), (2,3,4), (3,3,3), and (3,3,4). The agreement between the simulated and experimental data is reasonable considering the simplicity of the triangular distributions employed for the bond lengths, bend angles, and alignment functions, as shown in Figs. 4(a), 4(b), and 4(c). The presence of extra signal in the experimental momentum maps about the 0° and 180° positions when compared to simulation is likely to result from the time-of-flight degeneracy of the O^{4+} and C^{3+} ions. As with CO_2, the peak in the bond-length distribution indicates bonds that have been stretched to approximately double their equilibrium distance (R_{OC} 2.19 a.u. and R_{CS} 2.95 a.u.). This stretch is typical of a molecule of intermediate mass and is consistent with the rather well-established picture of critical distances and their importance through enhanced ionization that gives rise to a snapshot of molecular geometry during dissociation [13]. The bond-angle-distribution peaks at around 170° compared to the ground-state distribution that peaks at 175°, with the tail of the distribution stretching to 155°. The dashed line in Fig. 4(a) represents the maximum extent to which molecules with a linear geometry can be included in the distribution before a significant increase in the value of the least-squares fit is found; representing a measure of the sensitivity of fit. The above result is consistent with our previous finding in CO_2 [1] where straightening was not observed. In order to account

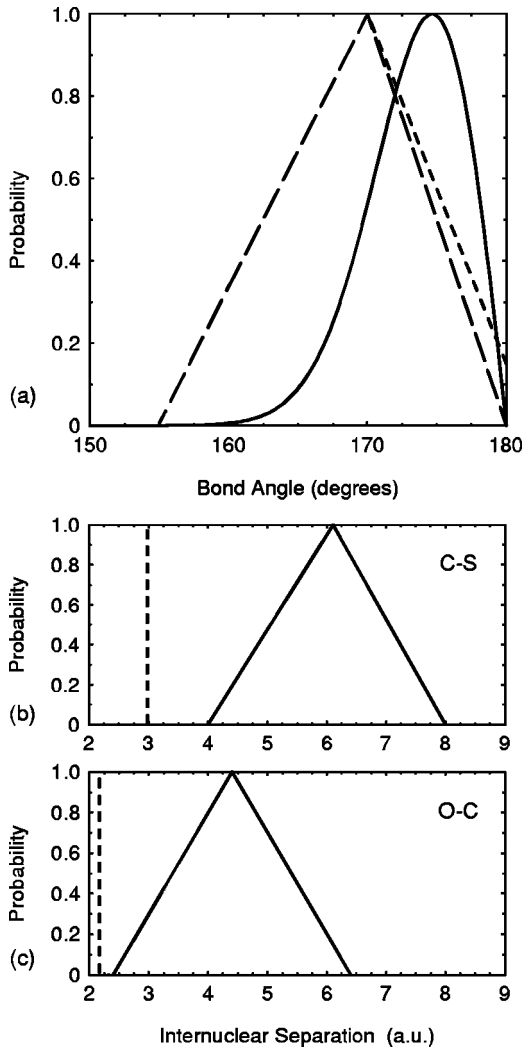

FIG. 4. (a) Simulated OCS bond-angle distribution (dashed line). The solid line represents ground-state zero-point distribution. The dotted line provides an upper bound on the presence of linear geometries. Corresponding simulated bond-length distributions for C-S and O-C branches of OCS are shown in (b) and (c), respectively, with dashed lines indicating equilibrium internuclear separation.

for the observations made for OCS we have performed single electron, over-the-barrier ionization calculations using a two-dimensional interaction potential calculated using a generalization of the method used by Posthumus *et al.* [14], in which the potential V at a point $\mathbf{r}$ is derived using

$$V(\mathbf{r}) = -\left(\sum_{i=1}^{3} \frac{Q_i}{\mathbf{r}-R_i}\right) - \varepsilon \cdot \mathbf{r}, \tag{3.1}$$

where Q_i is the charge state of the nucleus, ε is the laser electric field, and R_i is the nuclear separation from the electrostatic origin. Due to the geometric asymmetry of OCS this need not correspond to the location of the central atom as with CO_2. In this calculation the nuclear charges have not been averaged, as with earlier calculations [4,14], as the in-

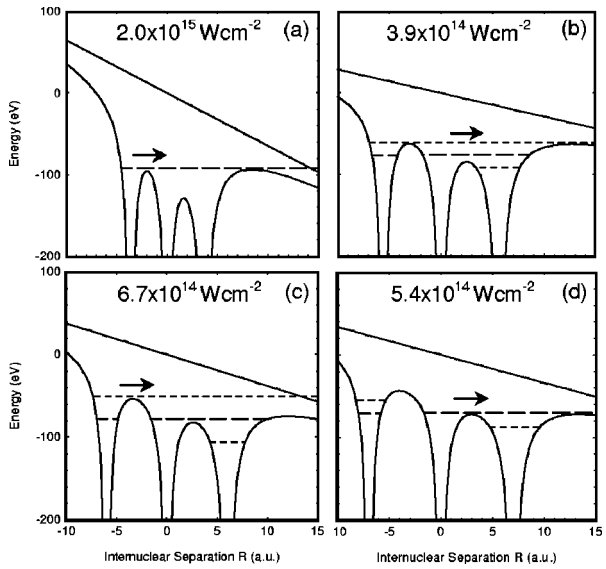

FIG. 5. Potential energy diagrams for OCS (3,3,4) showing (a) nonlocalized field ionization at the average molecular ionization potential (dashed line) at $R=3.70$ a.u., (b) ionization at critical internuclear separation at $R=5.85$ a.u., (c) electron localization in the oxygen well. The induced Stark shift (dotted lines) is sufficient for ionization at $R=6.00$ a.u., and (d) ionization from the central carbon well at $R=7.00$ a.u.

dividual nuclei may have quite different charges in the case of OCS. The nonlocalized electron energy level is calculated from

$$E=-\frac{1}{3}\left\{\sum_{i=1}^{3}\left[I_i+\sum_{j=1,j\neq i}^{3}\frac{Q_j}{R_{ij}}\right]\right\}, \tag{3.2}$$

where I_i is the ionization potential of the individual nucleus and R_{ij} is the internuclear separation. The effects of electron localization are substantially more complicated than in the diatomic case, where the energy level of the electron can be dc Stark shifted either up or down depending on which potential well it occupies. In the case of a triatomic molecule there are three wells in which the electron may be localized, in addition, the possibility of localization in a combination of middle and end well also exists. The shift in energy is simply given by the addition of the laser-field energy (assuming a dc approximation) at the center of the well in which the electron is localized, or the average of both wells when the electron is spread between them. The chance of ionization from localization in any well is further complicated by the possibility of unequal stretching of the O-C and C-S bonds, and so for simplicity these are only permitted to expand at an equal rate. Electron localization conditions are illustrated in Fig. 5 for the case of the laser electric field acting in the OCS direction (left to right in page). At small bond lengths, ionization is achieved only at high intensity and without electron localization, as shown in Fig. 5(a). As the bond length increases the electron ionizes from a localized position in the O well, as shown in Fig. 5(b), at the critical distance. With further increase in bond length the electron continues to be localized in the O well [Fig. 5(c)] until a region is encountered in which the molecule will preferentially ionize through localization in the C well [Fig. 5(d)], giving rise to a revival of enhanced ionization at larger R. This revival is similar in appearance to that predicted for the ionization rate of H_3^+ [15], which results from the variation of ionization pathway with internuclear separation using a tunneling approach. However, the present phenomenon is qualitatively different as it results purely from the assumption of electron localization.

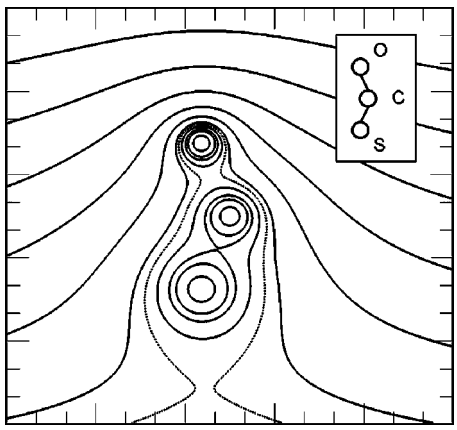

FIG. 6. Isopotential contour map of OCS (3,3,4) with a 140° bond angle at critical internuclear separation ($R=5.6$ a.u.) in an intense laser field ($I=3.9\times10^{14}$ W cm^{-2}) with the O-S bond aligned parallel to the laser polarization axis (vertical in page). The electron is shown to be localized in the oxygen well with ionization resulting from the induced Stark shift (dotted line).

By generalizing the calculations to two dimensions we can model the effect of the molecular bend on ionization [16]. Figure 6 shows the ionization of OCS with a bond angle of 140° into the (3,3,4) channel and illustrates how the electron escapes parallel to the laser polarization, but not along the bond axis. Before we can calculate the dependence of ionization threshold on bond angle, it is important to take into account the effects of orientation of OCS within the laser electric field, as the field direction changes in every cycle. Figure 7 shows the appearance intensity versus internuclear separation for the (3,3,4) channel for both linear and bent (90°) geometries. In each case the curves are derived from the average of O-C-S and S-C-O orientations in the field. The linear configuration shows the effect of the second enhanced ionization position at around 7 a.u., the importance of which is less than that of the first minimum, which is lower and therefore defines the critical distance at around 5.5 a.u. The ratio of the critical distance to the average equilibrium bond length $R_c/R_e=2.0$ agrees reasonably well with experimental results that give $R_c/R_e=1.9$. Interestingly, this calculation is closer to the experimental result than the calculation of Hishikawa *et al.* for CO_2 of $R_c/R_e=3.5$. The reason for the improved agreement in the present case seems to be the difference in the Z values of the molecular constituent atoms. The model only takes into account the change in attractiveness of the potential wells for the ionic charge state, and takes no account of different Z for each ion. However, the corresponding ionization potentials are dependent on the atom and are therefore Z specific, consequently the model is

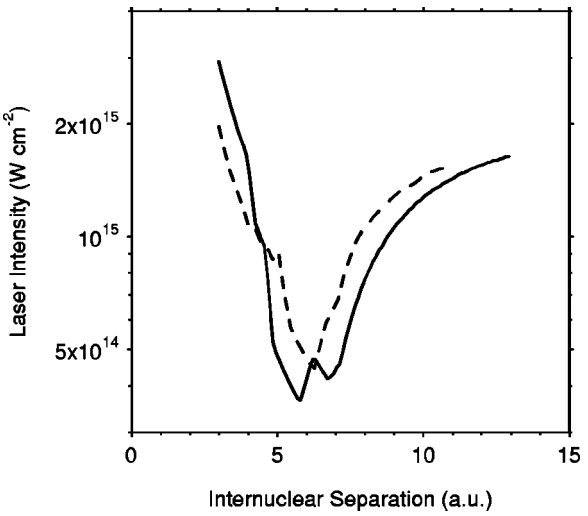

FIG. 7. Classical appearance-intensity curves for the OCS (3,3,4) channel with linear geometry (solid line) and a 90° bond angle (dashed line). In both cases the O-S bond is aligned along the laser polarization axis, with calculations averaged over both parallel and antiparallel orientations.

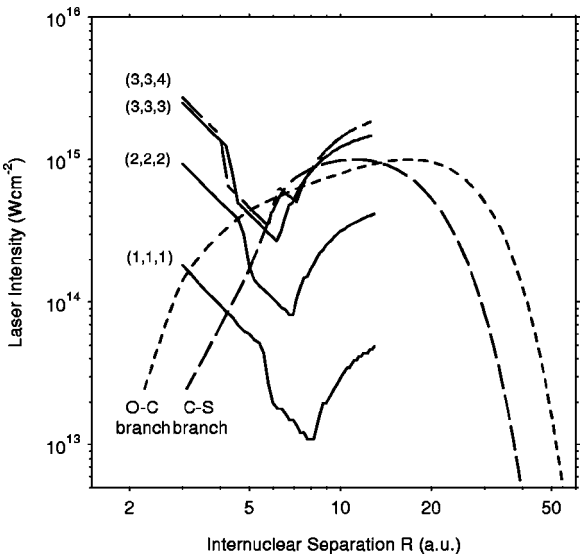

FIG. 8. Classical pulse trajectories for the O-C branch (dotted line) and C-S branch (dashed line) showing the evolution of the OCS molecular ion throughout the laser pulse. The trajectory is initiated by instantaneous removal of a nonlocalized electron, forming the channel $OCS^+(0.20,0.17,0.63)$. Subsequent dynamics result from modeling of the three-body Coulombic interaction during the evolving pulse. Trajectories intersect the (3,3,4) appearance-intensity curve at $R_{OC}=4.9$ a.u. and $R_{CS}=5.9$ a.u.

good for high Z where the many electrons are treatable statistically, but for light molecules the ionization potentials are shifted to higher values due to the lack of electron screening. The effect of the molecular geometry can be seen by comparing the appearance-intensity variation for the bent and straight molecules, the difference in the values at the critical distance is only a factor of 1.2, thus there is no great effect of geometry on appearance intensity. The overall conclusion that may be drawn from our calculations is that there is no strong correlation between bond angle and ionization rate for moderate bending $(180°-120°)$. The significance of this is that it means the measured geometry distributions are representative of the full range of molecular shapes that occur during dissociation of the variously charged molecules. This is important as it allows imaging of the molecular geometry without bias due to a variation of ionization threshold with molecular geometry. This relative independence of ionization threshold with moderate bond angles has also been predicted for H_3^{2+} under a parallel polarized field using a fully quantum-mechanical approach [17].

The purpose of developing these threshold curves is to model quantitatively the changing molecular geometry throughout the laser-pulse. In order to do this, we first have to decide on the starting conditions and subsequently allow the molecule to evolve freely within the laser pulse envelope. In the case of a diatomic molecule [4] this is fairly straightforward as only the initial dissociative conditions need to be decided upon along with the threshold intensity for the process. In the case of a triatomic molecule the additional constraint of initial molecular geometry is also present. In this instance the model starts from the singly charged molecular ion OCS^+ with the the threshold intensity for primary ionization calculated classically from the known molecular ionization potential [18]; however, this gives an intensity too high for the (1,1,1) channel to occur. This is because the molecule may ionize through multiphoton processes at much lower intensity than is necessary for field ionization. The threshold for the simulation was therefore set to 10^{13} W cm^{-2}. Even at this low threshold, the trajectory still crosses the (3,3,4) curve on the rising edge of the laser pulse for a peak intensity of 10^{15} W cm^{-2}. Final fragment energies have been found to be strongly dependent only on the final-ionization-threshold curve crossed, and therefore are largely independent of initial conditions, as it must be possible to reach the final observed ionization channel, in this case (3,3,4), from a range of initial geometries. This is how the mechanism of enhanced ionization itself chooses the temporal and spatial boundaries that give rise to a particular charge state.

The initial geometry for enhanced ionization calculations was chosen from within the range specified by the zero-point motion shown in Fig. 4(a), whereas the initial charge distribution was chosen to model the ''pre-Coulombic'' explosion dynamics of OCS^+ in a manner similar to that adopted by Hsieh and Eland [19]. The charge on the molecular ion was distributed unevenly, as if to form a channel (Q_1,Q_2,Q_3) where Q_i are fractions representing the degree of charge localization on each atom such that $\Sigma Q_i=1$. The charged fragments are then allowed to repel each other Coulombically. The geometry evolution was calculated within the changing laser-pulse envelope and the charge state is subject to the ionization thresholds derived in Fig. 8. Evolution of the molecular geometry occurs under the fractional charge state until the bond trajectories intersect the (1,1,1) channel ionization threshold curve, after which the molecular ion evolves with integer charges up to the (3,3,4) channel in this case. For ease of calculation we have omitted the bond-angle dependence on ionization as we have shown it to be of secondary importance.

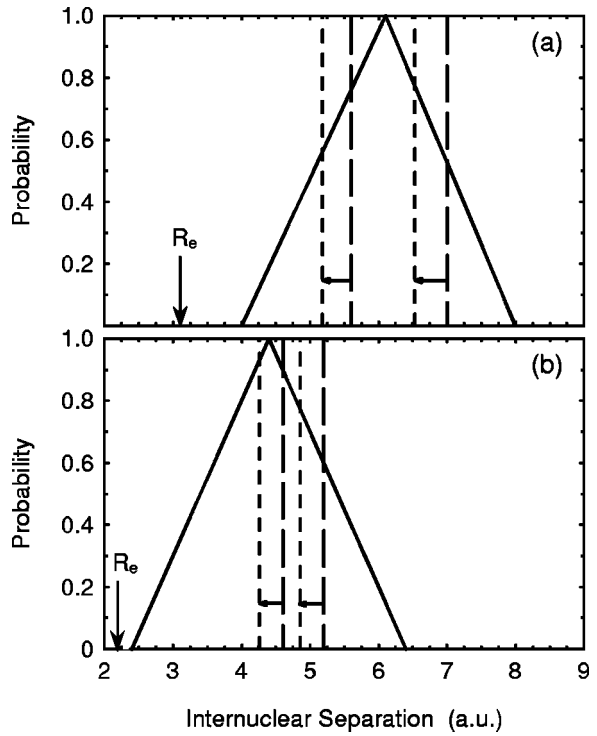

FIG. 9. Bond-length distributions for C-S (a) and O-C (b) branches, determined by Monte Carlo simulation (solid triangular) overlaid with limits determined from pulse-trajectory calculations (dashed lines). The dotted lines represent the equivalent limits under a static geometric approximation. Arrows indicate the position of equilibrium bond lengths.

Figure 8 shows the bond trajectories R_{OC} and R_{CS} for a molecule with an initial bond angle of 175°. In effect the bond trajectories are the 55-fs laser-pulse intensity profiles with the time ordinate transposed to internuclear separation, where the time transformation is derived from the Coulomb repulsion dynamics. By varying the pulse envelope within the parameters of our experimental pulse, we were able to find the range of peak intensities that result in the (3,3,4) channel, and hence the range of R_c for this ionization channel. This range can be compared directly to the R distributions obtained from the Monte Carlo simulation as shown in Fig. 9. The ranges are narrower than those obtained by Monte Carlo simulation and are also shifted to larger bond lengths, particularly for the O-C bond, however, the agreement is acceptable.

Now that we have the ability to calculate the trajectory of the fragment ions from pre-Coulombic, through the Coulombic interaction and on to infinity, the best measure of the fit of the trajectory calculation to our experiment is the asymptotic energy of the fragment ions. However, since the final quantities produced by the Monte Carlo simulation are bond-length and bond-angle distributions, it is convenient to use the static Coulomb explosion model to derive equivalent bond lengths and bond angles from the asymptotic energies obtained from the trajectory calculations. In this way we treat the trajectory results in the same way as the experimental data. The range of bond lengths derived in this way are also shown in Fig. 9 (dotted lines) alongside the simple pre-Coulombic and Monte Carlo results. As can be seen, the range of bond lengths are shifted back (as denoted by horizontal arrows in Fig. 9) into agreement with the original Monte Carlo distributions, in particular the range of O-C bond lengths is now very close to the peak predicted by the Monte Carlo simulation. This procedure indicates that the bond-length information obtained via Monte Carlo simulation is distorted towards shorter bond lengths as no account is taken of the pre-Coulombic energy.

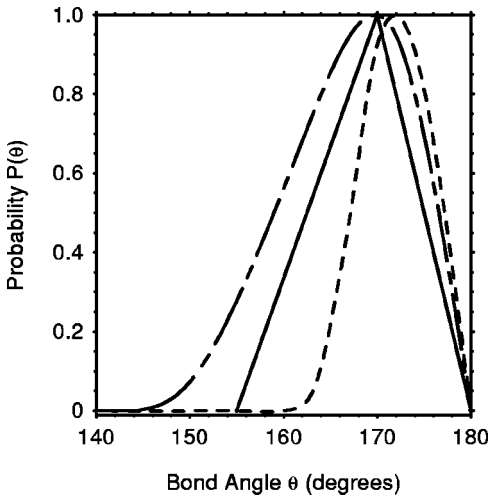

FIG. 10. Final Coulomb explosion bond-angle distributions as determined by Monte Carlo simulation (solid line), and the evolution of the zero-point distribution under the pre-Coulombic model (dot-dash line). The dashed line represents the apparent bond-angle distribution of the simulation when observed under the assumption of an initially static Coulomb explosion geometry, as employed by the Monte Carlo simulation.

In order to derive bond-angle information from the trajectory calculations complimenting the bond-length information discussed above, we start by taking a snapshot of the molecular ion at the critical distance. To do this we begin with an ensemble of molecules with instantaneous geometries corresponding to different positions on the zero-point bond-angle distribution. These are then allowed to expand and bend, ionizing as before when the trajectories cross the threshold curves. We can then map a distribution of bond angles at the critical internuclear separation from these evolved zero-point geometries. This is shown in Fig. 10 by the dot-dashed curve. Here we have chosen the initial charge distribution $OCS^+(0.20,0.17,0.63)$ that gives a best fit to the Monte Carlo bond-angle distribution. This charge distribution was chosen purely on quality of fit, however, it does have the virtue that the sulfur atom is the most positively charged fragment, in agreement with most observed final ionization channels. Once again this is only a first step, the fragment ions generated from this pre-Coulombic model must now be taken out to infinity, where the asymptotic energy can be determined, and used in the static Coulomb explosion model to determine the final molecular geometry. The results of this process are also presented in Fig. 10 as the dashed curve. Compared to the simple pre-Coulombic model (dot-dashed curve), the range of bond-angle geometries is

seen to narrow considerably. Although the peaks of the two distributions agree to within 2°, the low-angle tail of the equivalent static pre-Coulombic distribution straightens by over 15° compared to the simple pre-Coulombic model (162° rather than 147°). From this it is clear that the static model underestimates the amount of molecular bend present at the extreme of the distribution. Since the bond-angle distribution derived by the Monte Carlo simulation also utilizes this static approach, it must also underestimate the extent of bond-angle deformation that occurs prior to final Coulomb explosion. The Monte Carlo distribution already stretches to 155°, and it would most likely have to stretch another 15° to approximately 140° in order to reflect the true extent of the molecular bending.

The simple pre-Coulombic model is at the limit of what may be considered a reasonable charge distribution, so making the initial charge distribution more asymmetric is not an option. In order to explain the more bent geometries (155°–140°) it is tempting to invoke the effect of light-dressed potential energy surfaces (LDPES). This has previously been suggested as a possible reason for the straightening observed in H_2O, where the LDPES results from the one-photon coupling between the bent ground state $\tilde{X}^2B_1$ and the straight first excited state $\tilde{A}^2A_1$ of H_2O [2]. For NO_2 [6], one-photon coupling between a low-lying excited state and the ground state has been suggested to account for the observed straightening. Both these processes are feasible, however, such a process occurring in the neutral molecule seems unlikely, as deformation would have to occur extremely quickly on the very leading edge of the pulse prior to primary ionization.

The molecular geometries considered so far have all been bound, however, it is also important to consider the deformative effects of dissociative states. As we have shown in our simulation of a double dissociative process, this can lead to a significant increase in the bond angle at the critical internuclear separation. It may be that a combination of initial shape-changing transitions, either stable or dissociating, followed by ionization and concerted double dissociation can account for the difference between the observed and simulated bond-angle distribution. One candidate for such an initial process in OCS has recently been considered [22] involving rapid bending of the OCS molecule on the $1^1\Sigma^-$ and 1Δ states. This process results in a bond angle of around 135° in just 25 fs due to CO-S dissociation in which the CO-S bond length stretches by approximately 1 a.u. The molecule would need to undergo this single dissociative process for only a few femtoseconds to have the bond angle, but not bond length, significantly modified from the equilibrium ground-state value. Although excitation with near-IR radiation would require at least four photons, it does not require the implementation of any LDPES, and so could take place at low intensity, which is essential in order to occur within the neutral molecule.

IV. CONCLUSION

We have been able to image the OCS molecule during Coulomb explosion in an intense femtosecond laser pulse and, as previously observed in CO_2, we have seen evidence for molecular bending outside the zero-point range during enhanced ionization. By considering the pre-Coulombic motion of the OCS molecule we have been able to better test this enhanced ionization model. The bond lengths derived using this model have been shown to be in better agreement with experimental results when the pre-Coulombic motion is considered. Simulation of trajectories using a simple double dissociative process has shown that a broadening of the ground-state bond-angle distribution will occur, but that this broadening is insufficient to account for all experimentally observed geometries. We therefore suggest the presence of either LDPES or an initial single-bond (CO-S) bending dissociation, followed by double dissociation and subsequent Coulomb explosion.

ACKNOWLEDGMENT

This work was supported by the Engineering and Physical Sciences Research Council.

[1] W.A. Bryan, J.H. Sanderson, A. El-Zein, W.R. Newell, P.F. Taday, and A.J. Langley, J. Phys. B **33**, 745 (2000).
[2] A. Hishikawa, A. Iwamae, and K. Yamanouchi, J. Phys. B **28**, L723 (1995).
[3] S. Chelkowski, T. Zuo, A. Atabek, and A.D. Bandrauk, Phys. Rev. A **52**, 4, (1995).
[4] J.H. Posthumus, A.J. Giles, M.R. Thompson, and K. Codling, J. Phys. B **29**, 5811 (1996).
[5] J.H. Sanderson, A. El-Zein, W.A. Bryan, W.R. Newell, A.J. Langley, and P.F. Taday, Phys. Rev. A **59**, R2567 (1999).
[6] K. Yamanouchi, A. Hishikawa, A. Iwamae, and S. Lui, in *The Physics of Electronic and Atomic Collisions: XXI International Conference*, edited by Yukikazu Itikawa, Kazuhiko Okuno, Hiroshi Tanaka, Akira Yagishita, and Michio Matsuzawa, AIP Conf. Proc. No. 500 (AIP, Melville, NY, 2000).
[7] A. Hishikawa, A. Iwamae, K. Hoshina, M. Kono, and K. Yamanouchi, Chem. Phys. Lett. **282**, 283 (1998).
[8] M.D. Sturge, Solid State Phys. **20**, 92 (1967).
[9] G. Herzberg, Elec. Spectra of Polyatomic Molecules (Van Nostrand, New York, 1966).
[10] W.S. Struve, *Fundamentals of Molecular Spectroscopy* (Wiley, New York, 1989).
[11] W.C. Wiley and I. H. McLaren, Rev. Sci. Instrum. **26**, 1150 (1955).
[12] L.J. Frasinski, K. Codling, and P.A. Hatherly, Science **246**, 1029 (1989).
[13] K. Codling, J.H. Posthumus, and L.J. Frasinski, in *The Physics of Electronic and Atomic Collisions: XXI International Conference* (Ref. [6].
[14] J.H. Posthumus, L.J. Frasinski, A.J. Giles, and K. Codling, J. Phys. B **28**, L349 (1995).
[15] I. Kawata, H. Kono, and A.D. Bandrauk, Phys. Rev. A **64**, 043411 (2001).

[16] J.H. Posthumus, J. Plumridge, M.K. Thomas, K. Codling, L.J. Frasinski, A.J. Langley, and P. F. Taday, J. Phys. B **31**, L553 (1998).
[17] A.D. Bandrauk and J. Ruel, Phys. Rev. A **59**, 3 (1999).
[18] R. Feng, G. Cooper, Y. Sakai, and C. E. Brion, J. Chem. Phys. **255**, 353 (2000).
[19] S. Hsieh and J. H. Eland, J. Phys. B **30**, 4515 (1997).
[20] C. Cornaggia, M. Schmidt, and D. Normand, J. Phys. B **27**, L123 (1994).
[21] C. Cornaggia, Phys. Rev. A **54**, 4 (1995).
[22] T. Suzuki, H. Katayanagi, S. Nanbu, and M. Aoyagi, J. Chem. Phys. **109**, 5778 (1998).